PHYSICAL REVIEW A **75**, 041802(R) (2007)

Spatial Raman solitons in far-off resonant atomic systems

D. D. Yavuz
Department of Physics, University of Wisconsin at Madison, 1150 University Avenue, Madison, Wisconsin 53706, USA
(Received 12 January 2007; published 30 April 2007)

We predict two-frequency spatial optical solitons formed in atomic systems where a Raman transition is adiabatically prepared near a maximally coherent state. Using numerical simulations, we demonstrate the stability of these solitons against perturbations and investigate soliton-soliton collision properties.

DOI: 10.1103/PhysRevA.75.041802 PACS number(s): 42.50.Gy, 42.65.Tg, 42.65.Jx

Since the original suggestions of self-trapping for laser beams [1–3], there has been a growing interest in generation of spatial optical solitons due to their rich nonlinear dynamics, and their potential technological applications [4]. Over the last few decades, spatial optical solitons have been predicted and demonstrated in a variety of physical systems utilizing different nonlinear optical processes [5–9]. The formation of spatial optical solitons require a balance between the lensing effect of the medium and diffraction. In three spatial dimensions, it is well known that such a balance may be unstable, leading to collapse and filamentation of an optical wave [3].

An exciting practical application of spatial optical solitons is optical information processing. Collision processes between spatial solitons can be used to efficiently perform all-optical gates between laser beams. For such practical applications, there are several key challenges that have to be met: (1) The optical solitons for the studied physical system must be sufficiently stable to allow for well-defined collision properties, (2) the required optical power for each soliton must be low enough to keep the power requirement for a possible logic device within reasonable limits.

Recently, spatial Raman solitons formed in molecular systems were predicted [10,11]. In this Rapid Communication, we extend this suggestion and analyze the formation, propagation, and collision properties of spatial Raman solitons formed in far-off resonant atomic systems. Noting Fig. 1, the key idea is to drive a Raman transition with two laser beams whose frequency difference is slightly detuned from the frequency of the Raman resonance [12–15]. For sufficiently intense laser beams, almost half of the atomic population can be adiabatically transferred from ground Raman state $|a\rangle$ to excited Raman state $|b\rangle$. For this case, the magnitude of the coherence of the Raman transition (off-diagonal density matrix element) approaches its maximum value, $|\rho_{ab}| \approx 1/2$. The adiabatically prepared atomic coherence significantly modifies the refractive indices of the driving laser beams. Depending on the sign of the Raman detuning, $\Delta\omega$, the refractive indices of the driving laser beams are either enhanced ($\Delta\omega > 0$) or reduced ($\Delta\omega < 0$). This modification of the refractive index can cause self-focusing or self-defocusing of the driving lasers. As a result, under appropriate conditions, bright ($\Delta\omega > 0$) or dark ($\Delta\omega < 0$) two-frequency solitons are formed. Operating near maximum coherence, $|\rho_{ab}| \approx 1/2$, assures the stability of these solitons against perturbations and allows well-defined collision properties. As we will show below, spatial Raman solitons in atomic systems decisively meet the required criteria discussed in the previous paragraph.

Before proceeding we note that there is extensive literature on self-trapping and pattern formation of laser beams in atomic vapor cells utilizing one-photon resonances [16]. There has also been substantial work on electromagnetically induced focusing in a variety of near-resonance, two-frequency systems, including three level ladder, Λ, and V systems [17–22]. We begin by developing the formalism for a model atomic system, with two Raman states $|a\rangle$ and $|b\rangle$ and an arbitrary number of excited states $|i\rangle$, interacting with two driving lasers (termed the pump and the Stokes). We follow closely the formalism of Harris and colleagues [12–14]. Noting Fig. 1, we consider three-dimensional propagation of the driving lasers with electric field envelopes $E_p(x,y,z,t)$ and $E_s(x,y,z,t)$ such that the total field is $\hat{E}(x,y,z,t) = \mathrm{Re}\{E_p(x,y,z,t)\exp[j(\omega_p t - k_p z)] + E_s(x,y,z,t)\exp[j(\omega_s t - k_s z)]\}$ where $k_p = \omega_p/c$ and $k_s = \omega_s/c$. The two photon detuning from the Raman resonance is defined as $\Delta\omega = (\omega_b - \omega_a) - (\omega_p - \omega_s)$. When the two laser beams have the same polarization, new frequencies separated by the Raman transition (higher-order Stokes and anti-Stokes sidebands) will be generated as described in Refs. [13,14]. Throughout this paper, for simplicity, we will ignore these

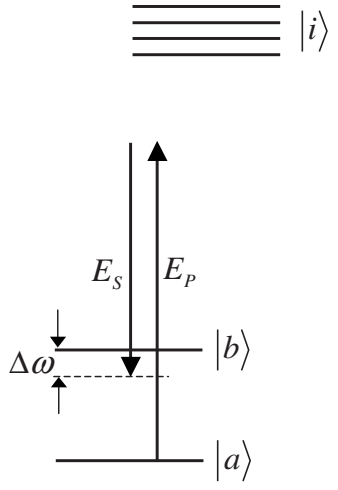

FIG. 1. Energy level diagram for a model atomic system. Two sufficiently strong laser beams, E_p and E_s, adiabatically prepare a maximally coherent atomic eigenstate. For $\Delta\omega > 0$, the atomic medium becomes self-focusing and bright two-frequency spatial solitons are formed.

additional frequencies. The generation of additional frequencies can, in principle, be prohibited by using frequency selective loss elements [23]. For a far-off resonant system where the detunings from one-photon resonances are large when compared with the inverse of the pulse width of the lasers, we can eliminate the derivatives of the probability amplitudes of the excited states $|i\rangle$. For this case, the temporal evolution of the probability amplitudes of states $|a\rangle$ and $|b\rangle$ is described by the following effective Hamiltonian [12–14]:

$$H_{\text{eff}}(x,y,z,t) = -\frac{\hbar}{2}\begin{bmatrix} A & B \\ B^* & D-2\Delta\omega \end{bmatrix}, \tag{1}$$

where $A=a_p|E_p|^2+a_s|E_s|^2$, $B=bE_pE_s^*$, and $D=d_p|E_p|^2+d_s|E_s|^2$. The constants a, b, and d determine the Stark shifts and the Raman coupling and are

$$a_{p,s} = \frac{1}{2\hbar^2}\sum_i \left[\frac{|\mu_{ai}|^2}{(\omega_i-\omega_a)-\omega_{p,s}}\right],$$

$$d_{p,s} = \frac{1}{2\hbar^2}\sum_i \left[\frac{|\mu_{bi}|^2}{(\omega_i-\omega_b)-\omega_{p,s}}\right],$$

$$b = \frac{1}{2\hbar^2}\sum_i \left[\frac{\mu_{ai}\mu_{bi}^*}{(\omega_i-\omega_a)-\omega_p}\right]. \tag{2}$$

Here, μ_{ij} are the dipole matrix elements between respective transitions. The Hamiltonian of Eq. (1) assumes the ideal case of zero linewidth for the Raman transition, and therefore, is valid for laser pulses short when compared with the inverse of the linewidth of the Raman resonance. When the elements of the effective Hamiltonian vary slowly when compared with the separation of the eigenvalues of the Hamiltonian, the atomic medium can be prepared adiabatically in an eigenstate that is smoothly connected to the ground state $|a\rangle$. The nature of preparation is similar to electromagnetically induced transparency (EIT) and coherent population trapping [24,25]. Defining $B=|B|\exp(j\varphi)$ and $\tan\theta=2|B|/(2\Delta\omega-D+A)$, the adiabatic solution for the density matrix elements are [12–14]

$$\rho_{aa} = \cos^2\left(\frac{\theta}{2}\right); \quad \rho_{bb} = \sin^2\left(\frac{\theta}{2}\right),$$

$$\rho_{ab} = \left(\frac{1}{2}\sin\theta\right)e^{j\varphi} = \text{sgn}(\Delta\omega)\frac{B/2}{\sqrt{|B|^2+(\Delta\omega-D/2+A/2)^2}}. \tag{3}$$

With the density matrix elements calculated by Eq. (3), the slowly varying envelope propagation equations for the pump and the Stokes beams in local time, $\tau=t-z/c$, are

$$2k_p\frac{\partial E_p}{\partial z} + j\frac{\partial^2 E_p}{\partial x^2} + j\frac{\partial^2 E_p}{\partial y^2} = -j2\eta\hbar\omega_p k_p N(a_p\rho_{aa}E_p + d_p\rho_{bb}E_p + b^*\rho_{ab}E_s),$$

$$2k_s\frac{\partial E_s}{\partial z} + j\frac{\partial^2 E_s}{\partial x^2} + j\frac{\partial^2 E_s}{\partial y^2} = -j2\eta\hbar\omega_s k_s N(a_s\rho_{aa}E_s + d_s\rho_{bb}E_s + b\rho_{ab}^*E_p), \tag{4}$$

where N is the atomic density and $\eta=(\mu/\epsilon_0)^{1/2}$. As also discussed in the introduction, in Eq. (3), the sign of ρ_{ab} is determined by the sign of the detuning, $\Delta\omega$. The first two terms on the right-hand side of Eq. (4) determine the refractive indices of the two laser beams in the absence of Raman interaction. The Raman coupling between the two laser beams is in the third term which contains the atomic coherence ρ_{ab}. The Raman refractive index effect can be qualitatively seen from these propagation equations. Depending on the phase of the atomic coherence, ρ_{ab}, the third term interferes either constructively or destructively with the first two terms resulting in refractive index enhancement or reduction. For the remainder of this paper, we will focus our attention to the bright soliton case ($\Delta\omega>0$), since it is easier to implement experimentally. In the numerical simulations presented below, we solve the propagation equations for the laser beams [Eq. (4)], together with the adiabatic solution for the density matrix elements [Eq. (3)] on a three-dimensional x-y-z spatial grid.

We proceed with soliton propagation and collision dynamics in a real atomic system. We choose our atomic medium to be ^{87}Rb vapor cell with an atomic density of $N=10^{14}$ cm^{-3}. The two Raman states are $|a\rangle\equiv|F=1,m_F=0\rangle$ and $|b\rangle\equiv|F=2,m_F=0\rangle$ hyperfine states of the ground electronic state $5S_{1/2}$. The frequency of the Raman excitation is therefore 6.834 GHz. We take both of the laser beams to be of the same circular polarization. We take the frequency of the pump beam E_p to be 100 GHz red detuned from the excited state $5P_{3/2}$ ($D2$ line). For such large one-photon detuning, the absorption of the beams due to the excited state while propagating through a 1-meter-long vapor cell is about 1% and is negligible. While calculating the constants a, b, and d, we include all relevant hyperfine states in the excited state manifold. The collisional dephasing linewidth for the Raman transition at $N=10^{14}$ cm^{-3} is $\gamma=2\pi\times11$ kHz. We take the two-photon detuning to be $\Delta\omega=2\pi\times10$ MHz, which is much larger than both the dephasing linewidth γ and also the two-photon Doppler linewidth. This assures the adiabatic preparation of atoms in all velocity classes. We also assume that the vapor cell is filled with a buffer gas of sufficient density (pressure larger than 100 torr) such that the diffusion of atoms across the spatial profiles of the beams is negligible for the time scales of interest ($1/\gamma\approx10$ μs).

We examine soliton stability and convergence by numerically propagating Gaussian spatial profiles with sufficient optical power. In Fig. 2, we plot one-dimensional cross sections for the intensity of the pump laser beam, $I_p=|E_p|^2/2\eta$, as a function of the propagation distance in the cell. In this simulation, the pump and the Stokes beams are assumed to have identical Gaussian spatial profiles with a Gaussian width of $w_0=100$ μm at the beginning of the cell. The integrated power in each beam is 130 mW, which corresponds to a peak intensity of 828 W cm^{-2} at the beginning of the cell. The peak value of the atomic coherence at the beginning of

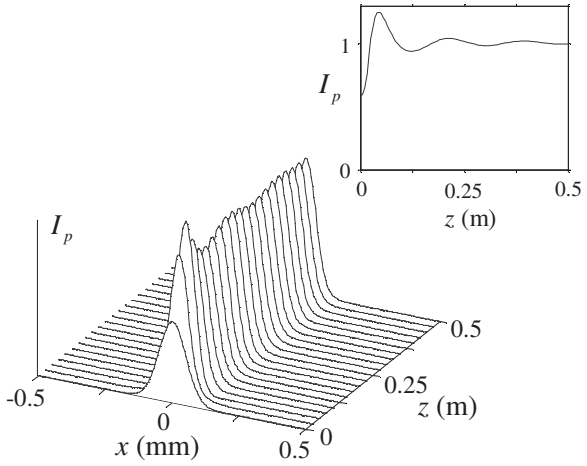

FIG. 2. Propagation of an initial Gaussian spatial profile through a 0.5-m-long atomic vapor cell. The plot shows one-dimensional slices of the intensity of the pump beam, $I_p=|E_p|^2/2\eta$, as a function of the propagation distance in the cell. After breathing, the profile converges to a soliton and propagates without further change. The Stokes beam shows an almost-identical behavior (not shown). The inset shows the normalized peak beam intensity as a function of propagation distance. In the absence of Raman self-focusing, the size of the beam would have increased by a factor of 12.5 due to diffraction.

the cell is $|\rho_{ab}|=0.44$. Noting Fig. 2, the spatial profile of the pump beam quickly converges to a soliton. The beam does not diffract and its spatial width is mostly maintained through 0.5 m of propagation along the vapor cell. The spatial profile of the Stokes beam also shows a very similar behavior (not plotted in Fig. 2). The inset in Fig. 2 shows the normalized peak intensity of the pump laser beam as a function of propagation distance along the cell detailing the convergence behavior. In the absence of Raman self-focusing, the beam size would have increased by a factor of 12.5 due to diffraction.

Figure 3 shows an elastic collision between two solitons where two solitons collide and pass through each other. Here, differing from the simulation of Fig. 2, we start with two Gaussian profiles for both laser beams propagating towards each other in the x-z plane with a collision angle of $\theta=4\times10^{-3}$ radians. Similar to Fig. 2, for each soliton, each of the pump and the Stokes beam has a power of 130 mW. In Fig. 3, we plot one-dimensional slices across the spatial profile of the pump beam as a function of the propagation distance. The solitons collide and pass through each other. The spatial profile of the Stokes beam shows a very similar behavior (not plotted in Fig. 3). The inset in Fig. 3 shows a contour plot for the intensity of the pump laser beam in the x-z plane.

Figure 4 shows an inelastic collision between two solitons where two solitons collide and fuse into a single soliton. Here, similar to Fig. 3, we start with two Gaussian profiles propagating towards each other in the x-z plane. However, we reduce the collision angle to $\theta=8\times10^{-4}$ radians such that each soliton cannot escape from the waveguide created by the other soliton. As a result, after substantial collision dynamics, the solitons fuse into each other.

The numerical simulations presented in Figs. 2–4 demonstrate the stability of Raman solitons against perturbations in

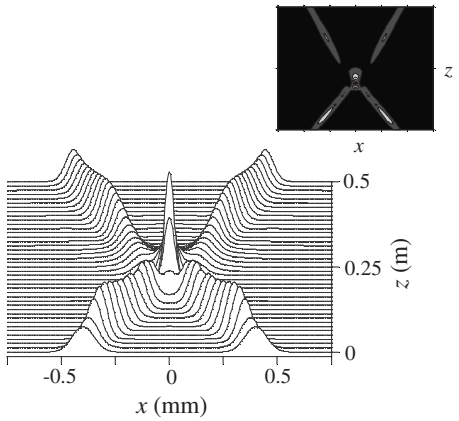

FIG. 3. An elastic collision between two solitons at a collision angle of $\theta=4\times10^{-3}$ radians. The plot shows one-dimensional slices of the intensity of the pump beam, $I_p=|E_p|^2/2\eta$, as a function of the propagation distance in the cell. The solitons collide, pass through each other, and continue propagating as solitons. The inset shows a contour plot of the same numerical simulation.

full three spatial dimensions. We now proceed with an analytical treatment to obtain insight into these results. For this purpose, we take the constants a, b, and d of Eq. (2) to be equal, $a_p=a_s=d_p=d_s=b$. We also take the Raman transition frequency to be much smaller than the frequencies of the driving lasers and therefore take $\omega_p=\omega_s$, $k_p=k_s$. For the numerical simulations of Figs. 2–4, these are valid assumptions. When the pump and the Stokes beams have identical boundary conditions at the beginning of the cell, $E_p(x,y,z=0)=E_s(x,y,z=0)$, the two propagation equations of Eq. (4) reduce to the same differential equation. Transforming $E_p(x,y,z)=E_s(x,y,z)=E(x,y,z)\exp(-j\eta\hbar\omega_p N a_p z)$ in Eq. (4), this differential equation is

$$2k_p\frac{\partial E}{\partial z}+j\frac{\partial^2 E}{\partial x^2}+j\frac{\partial^2 E}{\partial y^2}=-j\kappa\frac{|E|^2}{\sqrt{1+|b|^2|E|^4/\Delta\omega^2}}E, \quad (5)$$

where $\kappa=\eta\hbar\omega_p k_p N|b|^2/\Delta\omega$. For $|b||E|^2/\Delta\omega\ll1$ (unsaturated regime corresponding to $|\rho_{ab}|<0.1$), Eq. (5) reduces to the

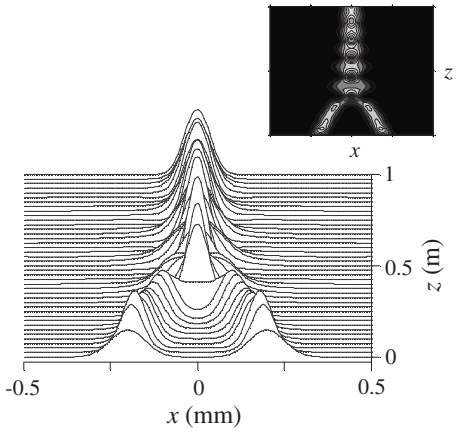

FIG. 4. An inelastic collision between two solitons at a collision angle of $\theta=8\times10^{-4}$ radians. The solitons collide and after substantial collision dynamics, fuse into each other. The inset shows a contour plot of the same numerical simulation.

well-known nonlinear Schrödinger equation. For this case, if we consider only one spatial transverse dimension, the well-known sech(…) bright soliton analytical solutions are immediately found. For two spatial dimensions, the soliton profiles can be found numerically [2]. In the saturated regime where $|\rho_{ab}| \approx 1/2$, even for single transverse dimension, the analytical solutions cannot be found and the profiles have to be calculated numerically [10,11]. The stability of spatial Raman solitons is a direct consequence of the saturation term on the right-hand side of Eq. (5) [26].

Throughout this work we have assumed an adiabatic density matrix solution for the atomic system. Since the nature of preparation is similar to front edge preparation of electromagnetically induced transparency [24], we expect a preparation energy requirement for spatial Raman solitons. This requirement states that the number of photons in the laser pulses must be large when compared with the number of atoms contained in the volume swept by the laser pulses, $V_{swept} = \frac{1}{2} L \pi w_0^2$, where L is the length of the medium [27]. For 10-μs-long laser pulses, this requirement is satisfied for the numerical simulations of Figs. 2–4. The calculation of the exact behavior requires time domain integration of the Schrödinger equation of Eq. (1) combined with the spatial integration of the propagation equations of Eq. (4), which is beyond our numerical capabilities at this moment. An exciting future direction would be to see if it is possible to combine spatial Raman solitons of this work with temporal Raman solitons [28–30] and to explore the possibility of observing light bullets (simultaneous trapping in space and time) [9]. Strongly driven Raman systems may be one of the few schemes where such light bullets can be observed.

To conclude, we predict a type of spatial optical solitons in strongly driven atomic systems. These solitons are substantially stable against perturbations and they have well-defined collision properties. They also require low optical powers (about 100 mW for the numerical simulations presented in Figs. 2–4) and therefore are ideally suited for optical information processing applications.

I would like to thank Nick Proite and Brett Unks for helpful discussions. This work was financially supported by the Department of Physics at University of Wisconsin-Madison.

[1] G. S. Askaryan, Sov. Phys. JETP **15**, 1088 (1962).
[2] R. Y. Chiao, E. Garmire, and C. H. Townes, Phys. Rev. Lett. **13**, 479 (1964).
[3] P. L. Kelley, Phys. Rev. Lett. **15**, 1005 (1965).
[4] G. I. Stegeman and M. Segev, Phys. Today **51**(8), 42 (1998); G. I. Stegeman and M. Segev, Science **286**, 1518 (1999).
[5] M. Segev, B. Crosignani, A. Yariv, and B. Fischer, Phys. Rev. Lett. **68**, 923 (1992).
[6] G. Duree *et al.*, Phys. Rev. Lett. **71**, 533 (1993).
[7] W. Torruellas *et al.*, Phys. Rev. Lett. **74**, 5036 (1995).
[8] A. Barthelemy, S. Maneuf, and C. Froehly, Opt. Commun. **55**, 201 (1985).
[9] Y. Silberberg, Opt. Lett. **15**, 1282 (1990).
[10] D. D. Yavuz, D. R. Walker, and M. Y. Shverdin, Phys. Rev. A **67**, 041803(R) (2003).
[11] M. Y. Shverdin, D. D. Yavuz, and D. R. Walker, Phys. Rev. A **69**, 031801(R) (2004).
[12] S. E. Harris, Opt. Lett. **19**, 2018 (1994).
[13] S. E. Harris and A. V. Sokolov, Phys. Rev. A **55**, R4019 (1997).
[14] S. E. Harris and A. V. Sokolov, Phys. Rev. Lett. **81**, 2894 (1998).
[15] D. R. Walker, D. D. Yavuz, M. Y. Shverdin, G. Y. Yin, A. V. Sokolov, and S. E. Harris, Opt. Lett. **27**, 2094 (2002).
[16] J. E. Bjorkholm and A. Ashkin, Phys. Rev. Lett. **32**, 129 (1974); G. Grynberg, A. Maitre, and A. Petrossian, Phys. Rev. Lett. **72**, 2379 (1994); R. S. Bennink, V. Wong, A. M. Marino, D. L. Aronstein, R. W. Boyd, C. R. Stroud, S. Lukishova, and D. J. Gauthier, *ibid.* **88**, 113901 (2002); B. Schapers, T. Ackeman, and W. Lange, IEEE J. Quantum Electron. **39**, 227 (2003).
[17] R. R. Moseley, S. Shepherd, D. J. Fulton, B. D. Sinclair, and M. H. Dunn, Phys. Rev. Lett. **74**, 670 (1995); Phys. Rev. A **53**, 408 (1996).
[18] J. T. Manassah and B. Gross, Opt. Commun. **124**, 418 (1996).
[19] A. G. Truscott, M. E. J. Friese, N. R. Heckenberg, and H. Rubinsztein-Dunlop, Phys. Rev. Lett. **82**, 1438 (1999).
[20] R. Kapoor and G. S. Agarwal, Phys. Rev. A **61**, 053818 (2000).
[21] T. Hong, Phys. Rev. Lett. **90**, 183901 (2003).
[22] H. Shpaisman, A. D. Wilson-Gordon, and H. Friedmann, Phys. Rev. A **71**, 043812 (2005).
[23] For the numerical simulations of Figs. 2–4, one can use two-photon Raman loss in an isotope specie, ^{85}Rb, and therefore selectively attenuate the generated first Stokes and anti-Stokes sidebands. This will prohibit generation of additional frequencies. In molecular systems [10,11], this problem is overcome by using opposite circularly polarized laser beams and thereby prohibiting additional sideband generation due to angular momentum selection rules. In far-off resonant alkali atoms, however, we cannot use this technique, since Raman coupling vanishes for opposite circularly polarized laser beams.
[24] S. E. Harris, Phys. Today **50** (7), 36 (1997).
[25] M. O. Scully and M. S. Zubairy, *Quantum Optics* (Cambridge University Press, Cambridge, 1997).
[26] N. G. Vakhitov and A. A. Kolokolov, Sov. Radiophys. **16**, 1020 (1973); J. J. Rasmussen and K. Rypdal, Phys. Scr. **33**, 481 (1986); J. M. Soto-Crespo, D. R. Heatley, E. M. Wright, and N. N. Akhmediev, Phys. Rev. A **44**, 636 (1991); J. M. Soto-Crespo, E. M. Wright, and N. N. Akhmediev, *ibid.* **45**, 3168 (1992).
[27] S. E. Harris and Z. F. Luo, Phys. Rev. A **52**, R928 (1995).
[28] A. E. Kaplan, Phys. Rev. Lett. **73**, 1243 (1994).
[29] K. Druhl, R. G. Wenzel, and J. L. Carlsten, Phys. Rev. Lett. **51**, 1171 (1983).
[30] D. V. Skryabin, F. Biancalana, D. M. Bird, and F. Benabid, Phys. Rev. Lett. **93**, 143907 (2004).